Biophysical *Journal*
Article

Biophysical Society

Hydrodynamic Hunters

Hossein Jashnsaz,[1] Mohammed Al Juboori,[2] Corey Weistuch,[3,4] Nicholas Miller,[2] Tyler Nguyen,[5] Viktoria Meyerhoff,[6] Bryan McCoy,[7] Stephanie Perkins,[8] Ross Wallgren,[9] Bruce D. Ray,[1] Konstantinos Tsekouras,[1] Gregory G. Anderson,[8,*] and Steve Pressé[1,7,10,*]

[1]Department of Physics and [2]Biomedical Engineering, Indiana University - Purdue University Indianapolis (IUPUI), Indianapolis, Indiana; [3]Department of Applied Mathematics and Statistics and [4]Department of Biochemistry and Cell Biology, Stony Brook University, Stony Brook, New York; [5]Stark Neurosciences Research Institute, Indiana University School of Medicine (ISUM), Indianapolis, Indiana; [6]Mechanical Engineering, [7]Department of Chemistry and Chemical Biology, [8]Department of Biology, and [9]Department of Mathematical Sciences, Indiana University - Purdue University Indianapolis (IUPUI), Indianapolis, Indiana; and [10]Cellular and Integrative Physiology Department, Indiana University School of Medicine (IUSM), Indianapolis, Indiana

ABSTRACT The Gram-negative *Bdellovibrio bacteriovorus* (BV) is a model bacterial predator that hunts other bacteria and may serve as a living antibiotic. Despite over 50 years since its discovery, it is suggested that BV probably collides into its prey at random. It remains unclear to what degree, if any, BV uses chemical cues to target its prey. The targeted search problem by the predator for its prey in three dimensions is a difficult problem: it requires the predator to sensitively detect prey and forecast its mobile prey's future position on the basis of previously detected signal. Here instead we find that rather than chemically detecting prey, hydrodynamics forces BV into regions high in prey density, thereby improving its odds of a chance collision with prey and ultimately reducing BV's search space for prey. We do so by showing that BV's dynamics are strongly influenced by self-generated hydrodynamic flow fields forcing BV onto surfaces and, for large enough defects on surfaces, forcing BV in orbital motion around these defects. Key experimental controls and calculations recapitulate the hydrodynamic origin of these behaviors. While BV's prey (*Escherichia coli*) are too small to trap BV in hydrodynamic orbit, the prey are also susceptible to their own hydrodynamic fields, substantially confining them to surfaces and defects where mobile predator and prey density is now dramatically enhanced. Colocalization, driven by hydrodynamics, ultimately reduces BV's search space for prey from three to two dimensions (on surfaces) even down to a single dimension (around defects). We conclude that BV's search for individual prey remains random, as suggested in the literature, but confined, however—by generic hydrodynamic forces—to reduced dimensionality.

INTRODUCTION

The Gram-negative bacterium *Bdellovibrio bacteriovorus* (BV) (1) is a model bacterial predator found across diverse habitats (2). It is poised to help purify water and soil (3), degrade biofilms (4), and serve as a living antibiotic (5). Decades of research have elucidated many aspects of BV's behavior (1). BV has a biphasic life cycle that includes an attack phase and a free-living phase. During the attack phase, BV grows within its Gram-negative prey's periplasm, replicates and, in a dramatic lytic event reminiscent of a virus, releases its free-living (mobile) phase progeny in search of bacterial prey. Most recently, studies have identified factors involved in its attachment and entry into prey (6), its effectiveness in killing pathogens (4,5,7,8), and safety in animal models (9,10). The availability of BV's genome sequence (2) has spurred detailed study into BV's physiology and molecular regulation (11,12). Despite this work, it is still unknown whether BV specifically targets its Gram-negative prey or simply bumps into it at random (3,13–15).

Early bulk studies concluded that BV most likely collides with prey randomly in solution, showing no significant chemotactic response for prey concentrations below 10^8 cells/mL while, at higher prey concentrations, sensing of prey by BV was attributed to the lysis of prey cells (3,14). More recent studies have shown that chemotaxis plays a modest role, and that while BV infects some prey cells more efficiently than others (7), no single receptor on BV's prey has been identified as a point of attachment

Submitted November 2, 2016, and accepted for publication February 7, 2017.

*Correspondence: stevenpresse@gmail.com or ga2@iupui.edu

Nicholas Miller and Tyler Nguyen contributed equally to this work.

Viktoria Meyerhoff, Bryan McCoy, Stephanie Perkins, and Ross Wallgren contributed equally to this work.

Steve Presse's present address is Physics and School of Molecular Sciences, Arizona State University, Tempe, Arizona

Editor: Anatoly Kolomeisky.

http://dx.doi.org/10.1016/j.bpj.2017.02.011

(15). In fact, BV's attachment to *Salmonella spp.* and *Escherichia coli* is robust to various outer membrane mutants (15,16).

It is conceivable that BV's hunting strategy would appear random if it is receiving conflicting chemoattractant signals from multiple surrounding prey. However, when sufficiently close to any single prey, no distinctive statistical signature of a targeted (chemotactic) search by BV for its prey—for instance, a volcano (17) effect that is expected for predators sensing chemoattractant point sources—has been found (18). Chemical sensing by BV for its prey would require BV to sensitively detect its prey and perhaps even forecast its moving prey's future position.

On the other hand, it is known that bacteria respond to self-induced (19,20) as well as external (21) hydrodynamic flows. For example, *E. coli* shows flagellar-mediated circular motion due to self-induced hydrodynamic flows near surfaces (22–24) and swims counter to external flows (21). Our experimental results discussed below—recapitulated by hydrodynamic calculations—demonstrate that not only is fast moving BV strongly influenced by its own self-generated hydrodynamic fields, but that hydrodynamic effects are critical in allowing BV to locate its prey. Because BV is small (~0.5 μm) and swims rapidly (>50 μm/s) through solution, our results show that it violently perturbs its liquid environment. While the complex dynamical effects of the liquid environment's response have been widely investigated for inanimate microswimmers such as catalysts (25), the role of hydrodynamics in bacterial predator-prey interactions is new, to our knowledge.

MATERIALS AND METHODS

Media

Bacteria were grown in Nutrient Broth (NB: 1 g/L yeast extract, 5 g/L peptone, 3 g/L beef extract, 0.294 g/L $CaCl_2$, pH 7.6); Diluted Nutrient Broth (DNB: 0.1 g/L yeast extract, 0.5 g/L peptone, 0.3 g/L beef extract, 0.294 g/L $CaCl_2$, pH 7.6); or calcium HEPES (CaHEPES: 0.294 g/L $CaCl_2$, 5.94 g/L HEPES, pH 7.6), as indicated in the text.

E. coli culture

E. coli strain MG1655 (26,27) was grown overnight in NB at 37°C with shaking (180 rpm). For *E. coli* motility experiments, the culture was used within 1–3 h after removal from the shaker.

BV culture

We used *Bdellovibrio bacteriovorus* (BV) strain 109 (BV Stolp and Starr, ATTC No. 15143; American Type Culture Collection, Manassas, VA) for all experiments in this study, unless otherwise mentioned. Frozen BV stocks were thawed at room temperature, pelleted in a microcentrifuge at 10,000 rpm for 6 min, and resuspended in 3 mL CaHEPES. Cultures were incubated at 30°C for 3 h, fed with 1 mL 3-day-old *E. coli* (strain SM10) culture, then incubated again in the same conditions. BV motility experiments were done after 12 h.

Microscopy and tracking

Bacteria were imaged with an inverted microscope (Nikon, Melville, NY) using a 60× phase oil immersion objective. Forty-five-second videos were recorded and trajectories were manually tracked using NIS tracking software (Nikon). We ignored nonmobile bacteria everywhere. The bacteria often went in and out of focus due to z-plane motion. To restrict our tracking to specific planes, we stopped tracking when bacteria got slightly out of focus (± 1 μm within the focus plane). In Figs. 2 and 4 *B*, BV and *E. coli* were tracked only while in complete focus to ensure that trajectories represented bacteria on the exact focus plane (with an estimated error bar of $\Delta z \sim 1$ μm).

Sample preparation

To explore movement around beads, we used electrically neutral Sepharose CL-6B beads (cross-linked (CL) beads; Sigma-Aldrich, St. Louis, MO), electrically positive diethylaminoethyl (DEAE) Sepharose Fast Flow beads (DEAE beads; GE Healthcare Life Sciences, Marlborough, MA), and electrically negative Sulfopropyl (SP) Sepharose Fast Flow beads (SP beads; Sigma-Aldrich), with sizes (radii) of 5–150 μm. To prepare and add beads to slides with motile bacteria, 30 μL of bead stock solution was added to 1 mL CaHEPES in a microcentrifuge tube and was centrifuged at 6400 rpm for 5 min. The supernatant was then removed and CaHEPES was added to the beads up to 1 mL total in the microcentrifuge tube. These steps were repeated 2–3 times. After the third wash, beads were resuspended in 1 mL of DNB and added to the slides with DNB and motile bacteria solutions (1/3 beads, 1/3 DNB, 1/3 BV or *E. coli*). To construct walls, a drop of nitrocellulose polymer was sandwiched between a coverslip and a microscope slide. Under slight pressure of the coverslip, the polymer spreads (typical diameter ~0.5–2 cm). After curing, it forms a hard edge straight enough to be considered a wall on the length scale of an ~0.5 μm BV (or even ~1 μm *E. coli*). Healthy swimming BV or *E. coli* solutions were then introduced against the edge of the wall.

RESULTS AND DISCUSSION

Before investigating hydrodynamics, we first looked at the behavior of populations of active BV around individual *E. coli* as well as larger pellets of *E. coli* to study the effect of chemotaxis on BV's search for its prey. The results are shown in Fig. 1, which reveals no density enhancement (chemotaxis) of predator around an individual prey cell (Fig. 1, *A* and *B*). However, large chunks of prey cells chemotactically attracted BV (Fig. 1, *C* and *D*). Both of these results are in agreement with early bulk studies using chemotaxis assays suggesting that BV most likely collides with individual prey randomly in solution, showing no significant chemotactic response for prey concentrations below 10^8 cells/mL while, at higher prey concentrations, sensing of prey by BV was attributed to its probable attraction to cell lysate (3,14).

Next, to establish that BV is in fact influenced by its own self-generated hydrodynamic flow fields near surfaces, we monitored BV swimming parallel to flat surfaces (Fig. 2). As BV's single flagellum rotates, propelling its body forward, its body counterrotates. In doing so, we expect BV to generate hydrodynamic flows above and below its body consistent with what is known about microswimmers swimming parallel to flat surfaces while rotating along their long axis (19,22,24). In this circumstance, fluid friction at the

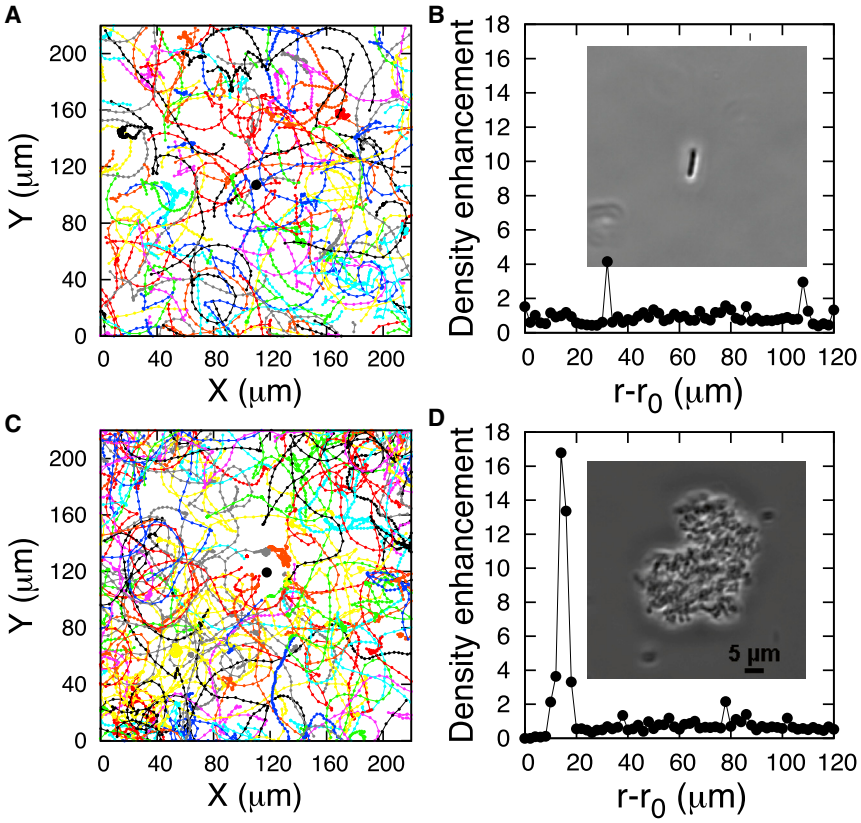

FIGURE 1 BV do not show chemotaxis toward individual *E. coli* although they do chemotactically accumulate around large chunks of *E. coli*. (*A*) Shows BV trajectories around an individual *E. coli* (whose location is designated by the *middle dot*). The density enhancement of BV is shown in (*B*) around the prey. (*C*) Shows the trajectories of BV around a large chunk of *E. coli*. The density enhancement of BV is shown in (*D*) around the chunk of prey. The insets in (*B*) and (*D*) show the microscope images of the individual *E. coli* and *E. coli* chunk; r_0 shows their geometric centers, respectively. The density enhancements in (*B*) is the density of motile BV with respect to the center of the individual *E. coli* computed at various distances from the *E. coli* divided by the average background density away from *E. coli* (see the Supporting Material for density calculation and Fig. S7). In (*D*), the only difference with (*B*) is that it is now the density of motile BV with respect to the geometric center of the chunk of *E. coli*. To create a chunk of *E. coli*, its overnight culture (see Materials and Methods) was centrifuged and the pellet suspended in CaHEPES, and a proper size piece of it was located under the microscope on a slide. To see this figure in color, go online.

surface (idealized as a no-slip boundary) induces a net force perpendicular to the swimmer's direction of motion. This, in turn, causes the swimmer to exhibit circular trajectories near surfaces. As we will discuss shortly, *E. coli* qualitatively behaves in the same way as BV although its flagellar physiology is completely different (*E. coli* has many flagella that bundle, while BV has just one). This suggests that the hydrodynamic forces described which act on the bacterium's body arise from the rotation of the body, not the details of the bacterial flagellar physiology.

In addition, we find that BV's trajectories show opposite helicities (clockwise versus counterclockwise rotation) on opposite surfaces (slide and coverslip, see Fig. 2 *A*) as would be expected if the circular trajectories were hydrodynamic in origin (Fig. 2, *B–H*; Movies S1, S2, and S3). Helicities are expected to switch if the flagellum predominantly rotates in one direction but the no-slip boundary condition is moved from below to above BV (see Fig. 2, *B* and *D*). Additionally, we confirmed that BV's flagellum rotates in one direction by monitoring BV tethered by its flagellum on a coverslip and tracking its body's rotation (Fig. S3).

While circular motion of bacteria may be caused by autochemotaxis (28), our data (Fig. 2, *B–H*) reveal a progressive loss of trajectory curvature as we move away from the surfaces and an eventual flip in helicity of BV's trajectories as we move past the midplane toward either the coverslip or the slide, consistent with hydrodynamic interactions and not autochemotaxis. Furthermore, by implementing a model presented in Spagnolie and Lauga (29) with boundary conditions consistent with those of our system, we can recapitulate both the helicity of the trajectory on surfaces and the increasing radius of curvature of those trajectories as we move away from the surface (Fig. 2 *J*); see Fig. S2 and the Supporting Material. Importantly, as we increase the viscosity of the solution, we saw the radius of the trajectories monotonically increase as would be expected if hydrodynamic effects weakened at higher viscosity (Fig. S4). While the component of the self-induced hydrodynamic flow parallel to the surface generates helicity in BV's trajectories near surfaces (22,24), the component perpendicular to the surface keeps bacteria close to the boundary, as shown in Fig. 2, *I* and *K*, where speed, dwell time, and length histograms show that hydrodynamics preferentially localize BV to regions near surfaces.

Many studies have investigated the accumulation of swimming microagents at flat surfaces including bacteria, algae, and artificial microswimmers (30–35). While this accumulation of microswimmers has been attributed to a number of different phenomena such as lubrication or near-field flows (25), persistent swimmer motion (34), or even contact interactions (32), our experimental results (Fig. 2), controls (Figs. S3 and S4), and numerical simulations (Fig. 2 *J*) discussed

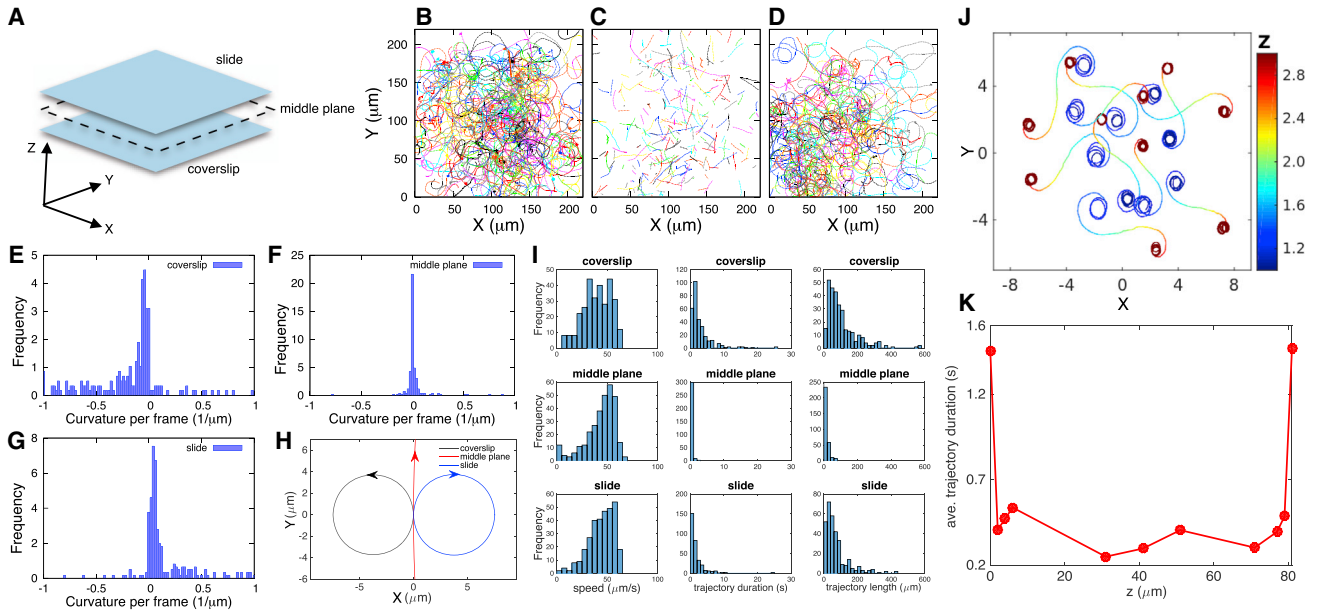

FIGURE 2 Self-generated hydrodynamic flows cause BV to interact strongly with surfaces. The motility of active BV was monitored at various planes between a microscope slide and a coverslip (*A*) separated by 40–90 μm (in such a way that the bacterium does not interact with surfaces when freely swimming through the middle plane). BV trajectories were recorded on the surface of the coverslip (*B*), the middle plane (*C*), and slide (*D*) (a sum of 290, 296, and 305 trajectories drawn from four samples, respectively). The signed curvature (helicity) histograms on the coverslip (*E*), middle plane (*F*), and slide (*G*) show a transition from counterclockwise to clockwise rotations. Positive curvature values indicate clockwise rotation, while negative curvature values indicate counterclockwise rotation. The helicity data are summarized in (*H*) by approximating trajectories as circles with the radius R_{eff} of $2/(\kappa_{\text{ave}} + \kappa_{\text{median}})$, where κ_{ave} and κ_{median} are the mean and median for the corresponding curvature histogram (see the Supporting Material for details of the calculation). The helicity of the circles on the surfaces depend on the bacterium's distance from the surface, the bacterium's shape, its propulsion mechanism, and the size and shape of the bacterium (29) (see the Supporting Material for detailed discussion). In addition, there are differences in the surface roughnesses that are reflected as slight differences in how bacteria interact with the coverslip and the microscope slide surface. These differences arise, for instance, because the coverslip has more debris while dead bacteria tend to stick to the slide. In (*I*), we show histograms of speed as well as duration and lengths of trajectories on each plane shown for those trajectories given in (*B*)–(*D*). Frequency in all plots represents trajectory count. (*J*) Hydrodynamic simulations from Spagnolie and Lauga (29)—adapted to match our boundary conditions—demonstrate that hydrodynamic interactions are sufficient to account for switching helicity (and trajectory radius size changes) as bacteria move between two surfaces with a z-range set arbitrarily between 1 and 3. BV dwell longer at the coverslip and microscope slide (0 being the coverslip plane), indicating that mobile BV is hydrodynamically forced onto surfaces (*K*). Each data point here represents the average dwell time of 20 trajectories recorded at that specific plane. Tracking criteria are explained in Materials and Methods. The helicity of all trajectories in figures in the main body and Supporting Material are opposite to the observations as seen in the movies (in other words, as seen from the coverslip side of our inverted setup). To see this figure in color, go online.

above suggest—in agreement with other recent studies on bacteria, e.g., Sipos et al. (30) and Berke et al. (31)—that hydrodynamic interactions dominate BV's behavior and dictate its accumulation on surfaces.

Next, we surmised that if the components of the hydrodynamic force induced by the swimming of BV perpendicular to the surface, along which BV swims, were important, then we should see BV preferentially swim along walls (30,35). Sample trajectories showing BV preferentially swimming along walls are shown in Fig. 3 with more data in Fig. S5.

Extending this logic to solid (chemically inert) beads as walls of finite radii, we should expect BV to be "geometrically captured" (25) in orbits around beads resting on the coverslip, with the dwell time of BV around the bead increasing with the bead's radius when capture is successful. This behavior, not yet observed to our knowledge in living organisms, would be consistent with the behavior of previously reported inanimate self-propelled Au-Pt particles (1, 2, and 4 μm) suspended in hydrogen peroxide solution captured in orbits closely following solid spheres (diameter 1–125 μm) (25).

To determine whether BV is geometrically captured, we explored mobile BV's behavior in the presence of inert (i.e., chemoattractant-free) and electrically neutral CL beads; see Materials and Methods and Fig. 3. We sandwiched active BV and CL beads—within a range of radii 20–60 μm—between a microscope slide and a coverslip (with sealed edges; see Fig. 3 *A*). Our results reveal that mobile BV orbits around beads (here of radius 56 μm) (Fig. 3 *C*; Movie S4), and shows a higher population density around them (Figs. 3 *D*, S6, and S7) by virtue of the same hydrodynamic forces that made BV swim along walls (Fig. 3 *B*) and generated higher densities of mobile BV near flat surfaces (Fig. 2). BV's density dramatically drops off to a background level within a few BV body lengths from the bead surface (~4–5 μm in

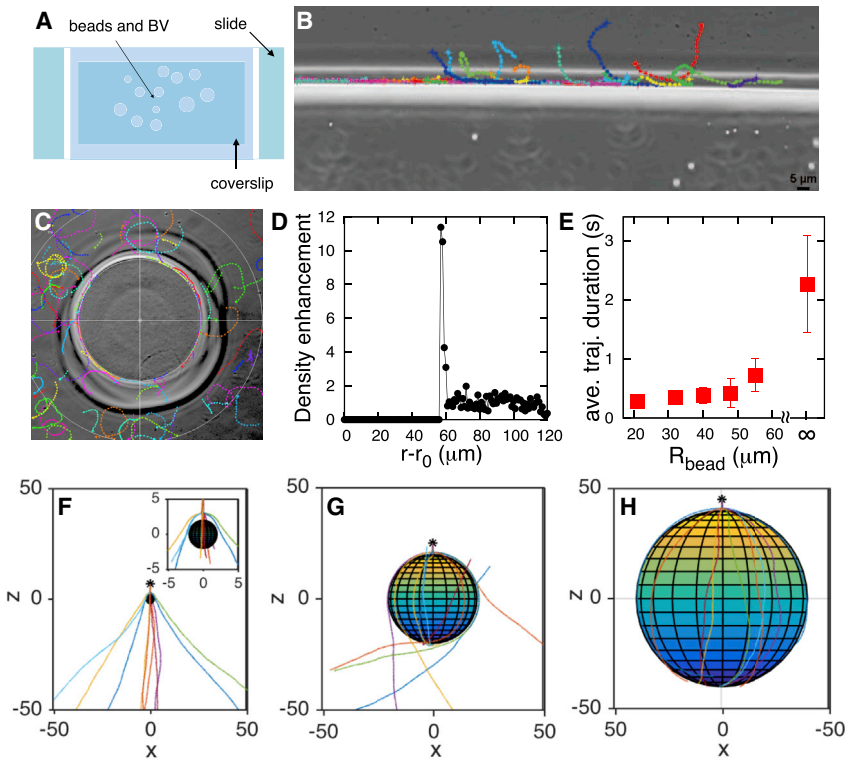

FIGURE 3 BV is geometrically captured in orbital motion around spherical inert beads. Active BV are mixed with inert CL beads between a microscope slide and a coverslip (*A*). Sample trajectories show BV swimming along a wall (constructed as explained in the Materials and Methods) (*B*), and being geometrically captured around beads (*C*). Each colored line indicates a separate bacterial trajectory, with the points along each line indicating the position of the bacterium at each interval. From 84 trajectories, we collected a density histogram (see the Supporting Material for details of the calculation) of BV showing how BV tightly localizes in orbital motion around beads (*D*). Density enhancement is computed with respect to the center of the bead (r_0) as explained in the Supporting Material and Fig. S7. Analysis of beads of decreasing size reveal how BV's capture time decreases for smaller beads (*E*). Each data point is the mean trajectory's duration within the capture region (5 μm from the bead surface) for a corresponding bead after dropping 5% of outliers from each side (that is, bacteria that stayed stuck to the bead or bacteria that only grazed the bead). The error bar is 1 SD. The data point corresponding to $R_{bead} = \infty$ shows the trajectory duration expected for an infinite radius bead (obtained by averaging the trajectory duration on the surface of the coverslip and slide combined; from Fig. 2, *B* and *D*). More data are provided in Figs. S6 and S7. Simulations of BV trajectories are shown around beads with radii of 2 (*F*), 20 (*G*), and 40 (*H*), measured in units of BV's bacterial body length with identical initial conditions. Model details are found in the Fig. S2 and the Supporting Material. The capture probability increases (from ~0 to ~1) as the bead size increases from 2 (*F*) to 40 (*H*). Strong interactions with the surface on which the bead rests contribute to BV's eventual detachment from the bead in experiments. To see this figure in color, go online.

Fig. 3 *D*). This means that beyond this typical distance, BV does not hydrodynamically interact with surfaces. This is in agreement with previous findings on self-generated bacterial flow field profiles for *E. coli*, which demonstrated that the flow field dissipates within a few bacterial body lengths from the cell (20).

Next, we eliminated the possibility that BV hunts by being geometrically captured by its prey. Experiments (Fig. 3 *E*) and simulations (Fig. 3, *F–H*, using a model adapted from Spagnolie et al. (36)) reveal that as we reduce the bead size ($\leq$40 μm), hydrodynamic forces no longer successfully capture BV. Furthermore, theory predicts (see Fig. S2 and the Supporting Material for details) that grazing trajectories become increasingly less curved as the size of the bead is reduced.

Because BV cells have electrically charged membranes, we assured ourselves that successful capture by larger beads is due to hydrodynamics and not possible residual electric charge on the beads we were using by monitoring BV's geometric capture around both positively charged (DEAE Sepharose Fast Flow) and negatively charged (SP Sepharose Fast Flow) beads (see details in Fig. S8). While BV is attracted to and eventually sticks to positive beads (therefore BV's surface is negatively charged), it still orbits around negatively charged beads, albeit more weakly, indicating that hydrodynamic interactions can even overcome weak electrostatic repulsion.

While BV is not successfully geometrically captured by objects as small as its bacterial prey, geometric capture by BV is a generic phenomenon that depends on: 1) the presence of an approximate no-slip boundary; and 2) the fact that BV's body rotates and thereby perturbs its liquid environment. We therefore hypothesize that its prey must also be susceptible to its own self-generated hydrodynamic fields and that these effects may passively colocalize predator and prey to improve the probability of chance collisions between BV and its prey. Thus, we repeated all experiments (on surfaces, along the wall, and around beads) with *E. coli*, a natural Gram-negative prey for BV (3). We found that *E. coli* also shows circling trajectories with opposite helicities on the coverslip and slide (Fig. 4 *A*), thereby confirming that *E. coli* is also influenced by its own self-induced hydrodynamic forces, consistent with Frymier et al. (23) and Lauga et al. (24). Fig. 4 recapitulates all the results for *E. coli* that were found for BV with walls and beads (Movie S5). In particular, we observed an enhancement of mobile density near solid objects, indicating geometric capture, and a density decrease 5–7 μm away from the bead's surface (compare with Fig. 3 for BV). We also repeated our controls with charged beads (with similar results) for *E. coli* (see Fig. S9).

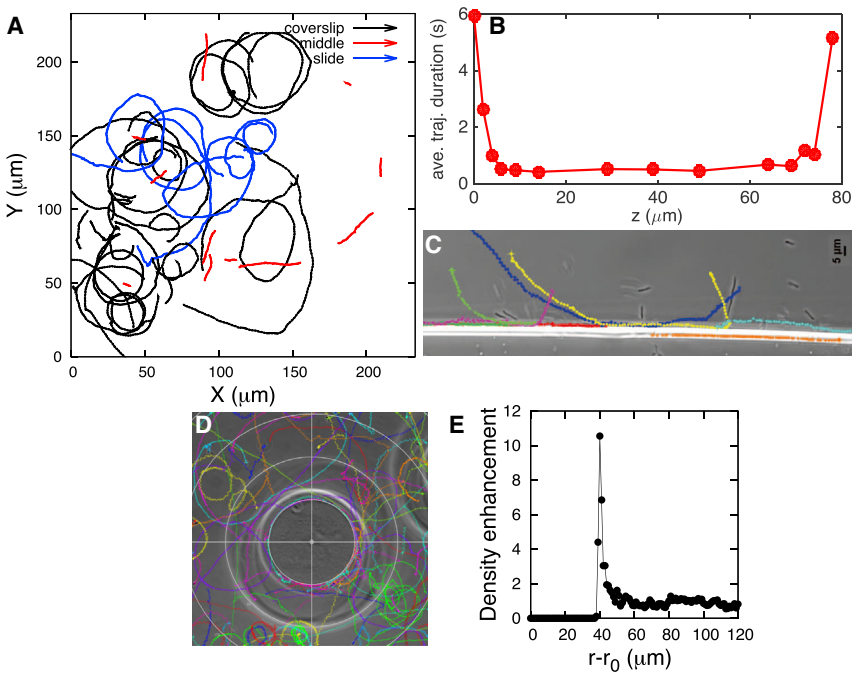

FIGURE 4 *E. coli* is also influenced by its own self-generated hydrodynamic fields. Like BV, *E. coli* circles on the coverslip and slide with opposite helicity (*A*), and sticks closely to surfaces and the wall (constructed as explained in Materials and Methods) (*B* and *C*). Based on a total of 24 trajectories of *E. coli* on the surfaces, we calculated a radius that was approximately twice as large as that of BV. This is expected from our hydrodynamic model as *E. coli* is longer than BV; based on our hydrodynamic model, longer bacteria make bigger circles on the surfaces (see the Supporting Material for detailed discussion). (*B*) Dwell time for trajectories recorded on each plane between a coverslip and a microscope slide, 0 being the coverslip plane. Like BV, *E. coli* is also geometrically captured by beads (*D*) (trajectories are recorded on the surface of the coverslip around the bead). Just as determined in Fig. 3 *D* for BV, mobile *E. coli* spends more time around the bead, showing enhanced density near the bead by contrast to regions away from the bead as seen in (*E*) (86 trajectories). To see this figure in color, go online.

We should point out that the large density of BV around the cluster of *E. coli* (Fig. 1 *D*) is not due to hydrodynamic forces. The cluster of *E. coli* that is used in this experiment is ~10 μm—much smaller than beads that successfully capture BV. Indeed, based on Fig. 3 *E* (experimental results) and Fig. S2 *B* (simulation results), the capture time for BV by a bead of radius 10 μm is negligible.

Our results thus show that hydrodynamic forces confine both predator and prey to surfaces (two-dimensional, 2D) and around defects on the surfaces such as small beads (one-dimensional, 1D), and we hypothesize that this in turn may increase the rate of random encounters between the predator and its prey. Fig. 5 shows the outcome of simulation for the encounter rates of the predator with the prey expected from our experimental results. Indeed, encounter times (times between two successive collisions) decrease dramatically from bulk solution (three-dimensional, 3D) to the surfaces (2D), and to the boundaries around the defects on the surfaces (1D). Furthermore, when considering the surface accumulation of the BV and *E. coli* near surfaces and along the defects (density enhancement due to hydrodynamic interactions), the decrease in the encounter time from 3D to 1D is even more pronounced (Fig. 5 *B*, *red circles* versus *black squares*). The overall effect is a reduction in encounter times between BV and *E. coli* especially pronounced at low densities (such as 0.125×10^6 pairs per mL; that is, one pair in (200 μm^3)) from hours to seconds. BV's life cycle includes an attack phase followed by a growth phase totaling 3–4 h (15). By contrast, *E. coli* has a much shorter life cycle (~0.5 h). Thus, while an encounter may make the difference between a successful and unsuccessful hunt for BV, it is only a drop in the bucket for the much more rapidly dividing *E. coli*. We hypothesize that this may be why BV has evolved to move quickly as its velocity makes it more susceptible to being affected by its own hydrodynamic forces.

CONCLUSIONS

While BV may be useful in targeting encapsulated prey that can otherwise resist eradication efforts (37), and may even serve as a living antibiotic by reducing bacterial infections in livestock (5), poultry (9), and possibly humans (38), the most basic features of BV's hunting strategy have remained elusive (15). In addition, BV has recently successfully been used in vivo in antibacterial therapy, suggesting this predatory bacterium as a promising candidate to fight antibiotic-resistant bacteria that present a serious rising concern (39). BV could have sought active prey by detecting chemotactic signals. However, because both predator and prey are active, not only would the predator have required high sensitivity to detect single prey but it may also have required the predator to forecast its prey's future position based on available information. Instead, our results provide, to our knowledge, a new perspective on bacterial predation that may explain why previous chemotactic studies of BV for its prey were inconclusive: Mobile BV use passive hydrodynamic forces to reduce their search space for prey from an undirected 3D search to an equally undirected search either confined to a surface or to a 1D motion around a large enough defect, thereby dramatically improving BV's odds of a chance

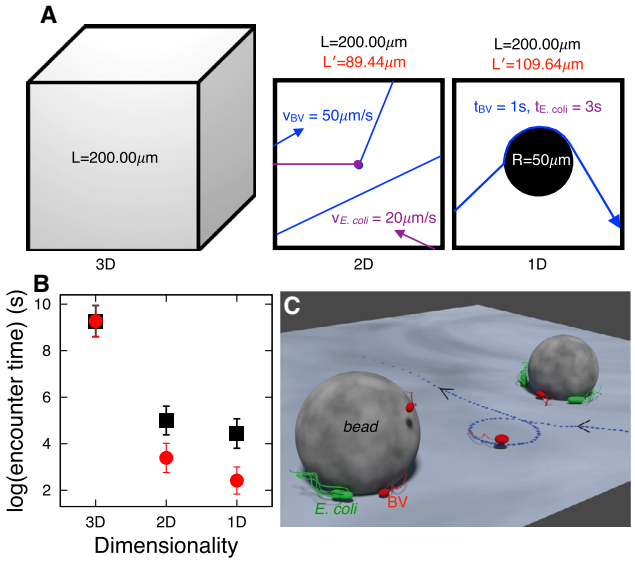

FIGURE 5 Hydrodynamic interactions, passively, enhance encounter rates of the predator with the prey. (*A*) Here we illustrate how we calculate the encounter rates of the predator with the prey using our experimental results. A cube of length $L = 200.00$ μm is considered to simulate encounter rates in 3D (*left*), the area of a square of the same length for 2D (*center*), and to capture the motion along the boundary of the beads on the surface of the coverslip, a circle of radius $R = 50$ μm inside the same square for 1D (*right*). A pair of BV and *E. coli*—with radii $r_{BV} = 0.50$ μm and $r_{E.coli} = 1.00$ μm (approximated as *spheres*)—initially start at the center of the cube and square and select a random direction, then move in straight paths with speeds of $v_{BV} = 50.00$ μm/s and $v_{E.coli} = 20.00$ μm/s (from experimental data, Fig. 2 *I*), respectively. When any of them collide with the surface of the cube (3D) or edge of the square (2D and 1D), they start from a new random position with a new random direction on a new random side of the cube or square (all uniformly). In the 1D case, they initially start from an arbitrarily point outside of the circle, and when they encounter the circle, they move along its circumference—BV for 1.0 s (Fig. 3 *E*) and *E. coli* for 3.0 s (averaged from 10 trajectories of *E. coli* along the bead surface on the coverslip) and then escape in a direction tangential to the circle. We record their positions at every 0.020 s (corresponding to a frame rate of 50 fps), and we consider a frame as an encounter time whenever the distance between BV and *E. coli* centers is less than $r_{BV} + r_{E.coli}$. We calculate encounter times from 1000 such collisions. (*B*) Natural logarithm of the encounter times (times between two successive encounters). (*Black squares*) Encounter times versus dimensionality without considering density enhancement (due to hydrodynamic effects); (*red circles*) corresponding times in the presence of the density enhancement. For red circles in 2D and 1D, we enhance the density fivefold to mimic density increases at surfaces due to hydrodynamics (Figs. 2 *K* and 4 *B*). We do so by reducing the length of the box from $L = 200.00$ μm to $L' = 89.44$ μm (2D) and to $L' = 109.64$ μm (1D). Error bars in (*B*) are 1 SD. (*C*) A qualitative illustration of geometric capture of predator and prey on surfaces and around beads as a result of their hydrodynamic interactions. To see this figure in color, go online.

collision. How these hydrodynamic effects could manifest themselves in vivo (39) as well as BV's natural habitat are the subject of future investigations. Our work may provide a starting point to investigate hydrodynamic effects on bacterial interactions that go beyond the chemical-sensing paradigm.

SUPPORTING MATERIAL

Supporting Materials and Methods, nine figures, and five movies are available at http://www.biophysj.org/biophysj/supplemental/S0006-3495(17)30218-7.

AUTHOR CONTRIBUTIONS

S. Pressé supervised all research and directed the theory; S. Pressé and G.G.A. codirected experiments; H.J., M.A.J., and N.M. performed all experiments; T.N., B.M., V.M., S. Perkins, and R.W. assisted in most experiments; B.D.R. provided technical support for experiments; H.J., C.W., K.T., and S. Pressé developed the theory; H.J., G.G.A., and S. Pressé wrote the article; and all authors participated in editing the article.

ACKNOWLEDGMENTS

S. Pressé acknowledges the National Science Foundation (NSF under grant No. MCB 1412259); G.G.A. acknowledges the National Institutes of Health (NIH under grant No. 1R03AR068724-01); and H.J. acknowledges a Graduate Student Imaging Research Fellowship from the Indiana University - Purdue University Indianapolis (IUPUI) Office of the Vice Chancellor for Research.

SUPPORTING CITATIONS

References (40–42) appear in the Supporting Material.

REFERENCES

1. Stolp, H., and M. P. Starr. 1963. *Bdellovibrio bacteriovorus* gen. et sp. n., a predatory, ectoparasitic, and bacteriolytic microorganism. *Antonie van Leeuwenhoek.* 29:217–248.
2. Rendulic, S., P. Jagtap, …, S. C. Schuster. 2004. A predator unmasked: life cycle of *Bdellovibrio bacteriovorus* from a genomic perspective. *Science.* 303:689–692.
3. Straley, S. C., and S. F. Conti. 1977. Chemotaxis by *Bdellovibrio bacteriovorus* toward prey. *J. Bacteriol.* 132:628–640.
4. Kadouri, D., and G. A. O'Toole. 2005. Susceptibility of biofilms to *Bdellovibrio bacteriovorus* attack. *Appl. Environ. Microbiol.* 71:4044–4051.
5. Boileau, M. J., K. D. Clinkenbeard, and J. J. Iandolo. 2011. Assessment of *Bdellovibrio bacteriovorus* 109J killing of *Moraxella bovis* in an in vitro model of infectious bovine keratoconjunctivitis. *Can. J. Vet. Res.* 75:285–291.
6. Lambert, C., I. T. Cadby, …, A. L. Lovering. 2015. Ankyrin-mediated self-protection during cell invasion by the bacterial predator *Bdellovibrio bacteriovorus*. *Nat. Commun.* 6:8884.
7. Rogosky, A. M., P. L. Moak, and E. A. Emmert. 2006. Differential predation by *Bdellovibrio bacteriovorus* 109J. *Curr. Microbiol.* 52:81–85.
8. Dashiff, A., R. A. Junka, …, D. E. Kadouri. 2011. Predation of human pathogens by the predatory bacteria *Micavibrio aeruginosavorus* and *Bdellovibrio bacteriovorus*. *J. Appl. Microbiol.* 110:431–444.
9. Atterbury, R. J., L. Hobley, …, R. E. Sockett. 2011. Effects of orally administered *Bdellovibrio bacteriovorus* on the well-being and *Salmonella* colonization of young chicks. *Appl. Environ. Microbiol.* 77:5794–5803.
10. Shatzkes, K., R. Chae, …, D. E. Kadouri. 2015. Examining the safety of respiratory and intravenous inoculation of *Bdellovibrio bacteriovorus* and *Micavibrio aeruginosavorus* in a mouse model. *Sci. Rep.* 5:12899.
11. Hobley, L., R. K. Fung, …, R. E. Sockett. 2012. Discrete cyclic di-GMP-dependent control of bacterial predation versus axenic growth in *Bdellovibrio bacteriovorus*. *PLoS Pathog.* 8:e1002493.

12. Rotem, O., J. Nesper, …, E. Jurkevitch. 2015. An extended cyclic di-GMP network in the predatory bacterium *Bdellovibrio bacteriovorus*. *J. Bacteriol.* 198:127–137.
13. Lambert, C., M. C. M. Smith, and R. E. Sockett. 2003. A novel assay to monitor predator-prey interactions for *Bdellovibrio bacteriovorus* 109 J reveals a role for methyl-accepting chemotaxis proteins in predation. *Environ. Microbiol.* 5:127–132.
14. Varon, M., and B. P. Zeigler. 1978. Bacterial predator-prey interaction at low prey density. *Appl. Environ. Microbiol.* 36:11–17.
15. Lambert, C., K. A. Morehouse, …, R. E. Sockett. 2006. *Bdellovibrio:* growth and development during the predatory cycle. *Curr. Opin. Microbiol.* 9:639–644.
16. Varon, M., and M. Shil. 1968. Interaction of *Bdellovibrio bacteriovorus* and host bacteria. I. Kinetic studies of attachment and invasion of *Escherichia coli* B by *Bdellovibrio bacteriovorus*. *J. Bacteriol.* 95:744–753.
17. Bray, D., M. D. Levin, and K. Lipkow. 2007. The chemotactic behavior of computer-based surrogate bacteria. *Curr. Biol.* 17:12–19.
18. Jashnsaz, H., T. Nguyen, …, S. Pressé. 2015. Inferring models of bacterial dynamics toward point sources. *PLoS One.* 10:e0140428.
19. Lauga, E. 2016. Bacterial hydrodynamics. *Annu. Rev. Fluid Mech.* 48:105–130.
20. Drescher, K., J. Dunkel, …, R. E. Goldstein. 2011. Fluid dynamics and noise in bacterial cell-cell and cell-surface scattering. *Proc. Natl. Acad. Sci. USA.* 108:10940–10945.
21. Kaya, T., and H. Koser. 2012. Direct upstream motility in *Escherichia coli*. *Biophys. J.* 102:1514–1523.
22. Hu, J., A. Wysocki, …, G. Gompper. 2015. Physical sensing of surface properties by microswimmers—directing bacterial motion via wall slip. *Sci. Rep.* 5:9586.
23. Frymier, P. D., R. M. Ford, …, P. T. Cummings. 1995. Three-dimensional tracking of motile bacteria near a solid planar surface. *Proc. Natl. Acad. Sci. USA.* 92:6195–6199.
24. Lauga, E., W. R. DiLuzio, …, H. A. Stone. 2006. Swimming in circles: motion of bacteria near solid boundaries. *Biophys. J.* 90:400–412.
25. Takagi, D., J. Palacci, …, J. Zhang. 2014. Hydrodynamic capture of microswimmers into sphere-bound orbits. *Soft Matter.* 10:1784–1789.
26. Kuchma, S. L., J. P. Connolly, and G. A. O'Toole. 2005. A three-component regulatory system regulates biofilm maturation and type III secretion in *Pseudomonas aeruginosa*. *J. Bacteriol.* 187:1441–1454.
27. Blattner, F. R., G. Plunkett, 3rd, …, Y. Shao. 1997. The complete genome sequence of *Escherichia coli* K-12. *Science.* 277:1453–1462.
28. Taktikos, J., V. Zaburdaev, and H. Stark. 2011. Modeling a self-propelled autochemotactic walker. *Phys. Rev. E Stat. Nonlin. Soft Matter Phys.* 84:041924.
29. Spagnolie, S. E., and E. Lauga. 2003. Hydrodynamics of self-propulsion near a boundary: predictions and accuracy of far-field approximations. *J. Fluid Mech.* 700:105–147.
30. Sipos, O., K. Nagy, …, P. Galajda. 2015. Hydrodynamic trapping of swimming bacteria by convex walls. *Phys. Rev. Lett.* 114:258104.
31. Berke, A. P., L. Turner, …, E. Lauga. 2008. Hydrodynamic attraction of swimming microorganisms by surfaces. *Phys. Rev. Lett.* 101:038102.
32. Li, G., and J. X. Tang. 2009. Accumulation of microswimmers near a surface mediated by collision and rotational Brownian motion. *Phys. Rev. Lett.* 103:078101.
33. Lee, C. F. 2013. Active particles under confinement: aggregation at the wall and gradient formation inside a channel. *New J. Phys.* 15:055007.
34. Elgeti, J., and G. Gompper. 2013. Wall accumulation of self-propelled spheres. *Europhys. Lett.* 101:48003.
35. Yazdi, S., A. M. Ardekani, and A. Borhan. 2015. Swimming dynamics near a wall in a weakly elastic fluid. *J. Nonlinear Sci.* 25:1153–1167.
36. Spagnolie, S. E., G. R. Moreno-Flores, …, E. Lauga. 2015. Geometric capture and escape of a microswimmer colliding with an obstacle. *Soft Matter.* 11:3396–3411.
37. Koval, S. F., and M. E. Bayer. 1997. Bacterial capsules: no barrier against *Bdellovibrio*. *Microbiology.* 143:749–753.
38. Sockett, R. E., and C. Lambert. 2004. *Bdellovibrio* as therapeutic agents: a predatory renaissance? *Nat. Rev. Microbiol.* 2:669–675.
39. Willis, A. R., C. Moore, …, R. E. Sockett. 2016. Injections of predatory bacteria work alongside host immune cells to treat Shigella infection in Zebrafish Larvae. *Curr. Biol.* 26:3343–3351.
40. Gabel, C. V., and H. C. Berg. 2003. The speed of the flagellar rotary motor of *Escherichia coli* varies linearly with protonmotive force. *Proc. Natl. Acad. Sci. USA.* 100:8748–8751.
41. Qian, C., C. C. Wong, …, K.-H. Chiam. 2013. Bacterial tethering analysis reveals a "run-reverse-turn" mechanism for *Pseudomonas* species motility. *Appl. Environ. Microbiol.* 79:4734–4743.
42. Swindells, J. F., C. F. Snyder, …, P. E. Golden. 1958. Viscosities of Sucrose Solutions at Various Temperatures: Tables of Recalculated Values. Supplement to National Bureau of Standards Circular, Vol. 440. National Bureau of Standards, Gaithersburg, MD, pp. 1–7.